First Year Report
and
Request for Renewal

of

Multiresolution and Explicit Methods for Vector Field Analysis and Visualization

National Aeronautics and Space Administration
Ames Research Center
NAS Systems Division, Code RNR
Moffett Field, CA 94035-1000
NRA2-36206(LMV)

Technical Contact: Gregory M. Nielson, CS&E, ASU, Tempe, AZ 85287-5406
(602) 965-2785, 962-6739, email: nielson@asu.edu

Introduction

This is a request for renewal of a research project which is concerned with the development of new and improved methods for:

- Multiresolution representation for very large, time-dependent, curvilinear grids with multiple masked overlapping blocks.

- Explicit methods for streamlines, stream surfaces and other flow field visualization methods.

In the following two sections we describe the current progress of the research project and a statement of the research work for next year.

Report on Current Progress

We first report on our current progress in the area of explicit methods for tangent curve computation. The basic idea of this method is to decompose the domain into a collection of triangles (or tetrahedra) and assume linear variation of the vector field over each cell. With this assumption, the equations which define a tangent curve become a system of linear , constant coefficient ODE's which can be solved explicitly. There are five different representation of the solution depending on the eigenvalues of the Jacobian. The analysis of these five cases is somewhat similar to the phase plane analysis often associate with critical point classification within the context of topological methods, but it is not exactly the same. There are some critical differences. Moving from one cell to the next as a tangent curve is tracked, requires the computation of the exit point which is an intersection of the solution of the constant coefficient ODE and the edge of a triangle. There are two possible approaches to this root computation problem. See Figure 1. We can express the tangent curve into parametric form and substitute into an implicit form for the edge or we can express the edge in parametric form and substitute in an implicit form of the tangent curve. Normally the solution of a system of ODE's is given in parametric form and so the first approach is the most accessible and straightforward. The second approach requires the "implicitization" of these parametric curves. The implicitization of parametric curves can often be rather

2

difficult, but in this case we have been successful and have been able to develop algorithms and subsequent computer programs for both approaches. We will give these details along with some comparisons in a forthcoming research paper on this topic.

Parametric Curve

Implicit Edge

P_i

$(x(t), y(t))$

P_j

$Ax(t) + By(t) + C = 0$

No Bracketing

$0 < t < ?$

Implicit Curve

Parametric Edge

P_i

$F(x, y) = 0$

$(1-t)\ P_i + t\ P_j$

P_j

$F(x(t), y(t)) = 0$

Bracketing

$0 \leq t \leq 1$
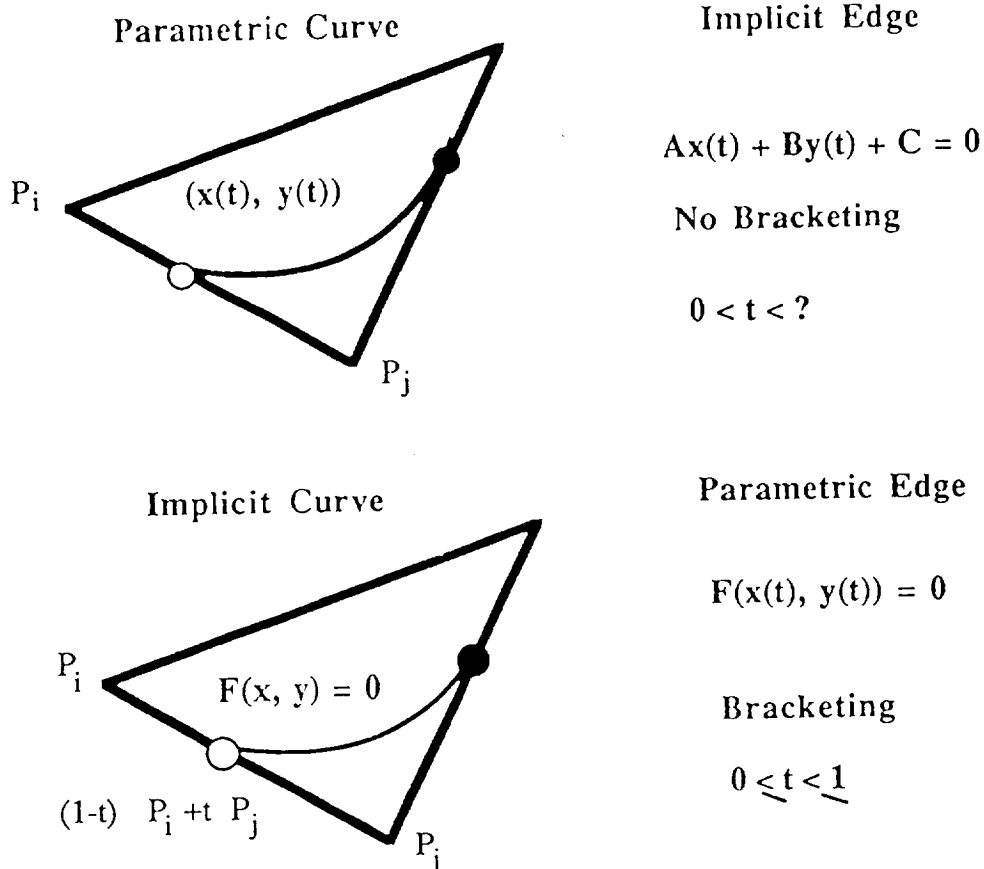
Figure 1. Two approaches to computing exit point.

We now include some examples illustrating the use of our new methods. In Figure 2, we show the topological graph of a simple vector field with is specified by the two equations. Since we know the exact solution in this case, we can apply our methods and see if they work at all and also see how well they approximate the true solution. We can vary the size and resolution of the grid in order to asses the rate of approximation. In the top image of Figure 2 we have used a 5x5 Cartesian grid with diagonals yielding triangles and in the bottom image we have use a 15x15 grid. The example of Figure 3 shows that these methods can be used on any domain which can be triangulated! Here we have a two-dimensional flow field defined over spherical domain which has been triangulated. In this particular case, the triangulations are obtained by subdivision and the right column is one more level of the subdivision than the left.

3

Each column shows three different rotations of the Earth. The blue curves represent the topological graph and the cyan curves are some additional tangent curves. In Figure 4, we show the topological graph of a two-dimension flow defined over a curvilinear grid which has an interior boundary. We include this example so that we might discuss the points of attachment and detachment on the interior boundary. The computation of this type of critical point has not been rigorously treated in the past. Within this context these points are precisely defined and easily computed. Without these points, the linking algorithm will leave some unattached foci and nodes in the domain. Note the connection between a focus point and a point of detachment in the lower left region. The details of this type of analysis and the improved linking algorithm will be included in the research paper we have already mentioned. In Figure 5, we show some results for a three-dimensional vector field. This is really preliminary work and we need to do a lot more in this area so as to make the algorithms efficient and robust, but the figure does show promise and the possibility to extend these methods to higher dimensions.

$$U(x,y) = \quad -0.103 + 0.052x - 0.303y$$
$$+ 0.038xy - 0.232x^2 + 0.612y^2$$

$$V(x,y) = \quad +0.143 + 0.688x - 0.145y$$
$$-0.213xy - 1.030x^2 + 0.246y^2$$
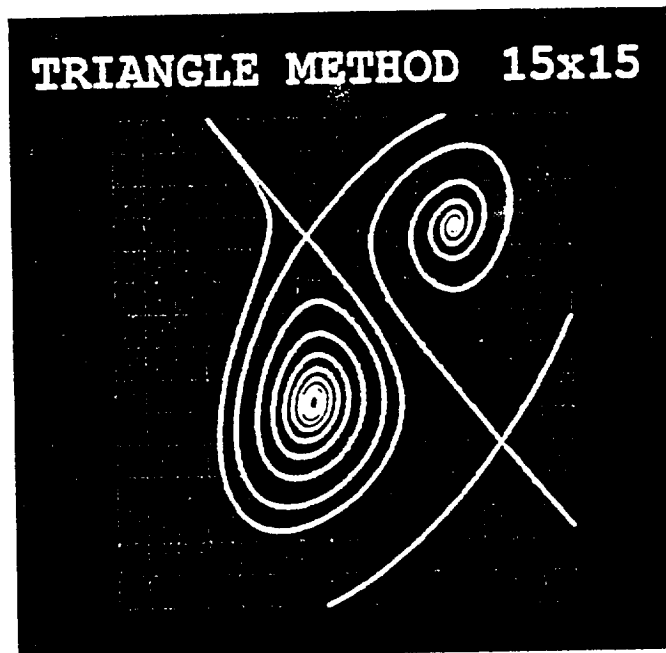
Figure 2. Flow data provided by an equation.
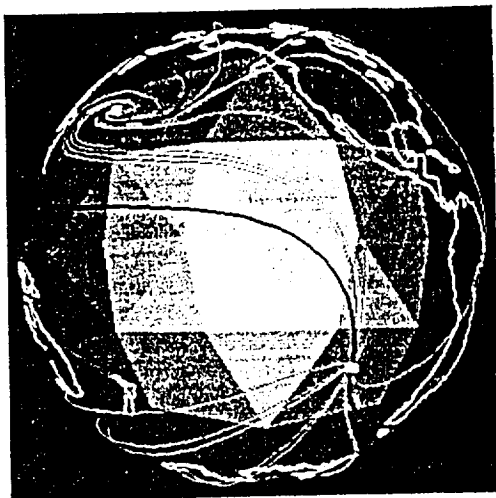
View 1. Level 3
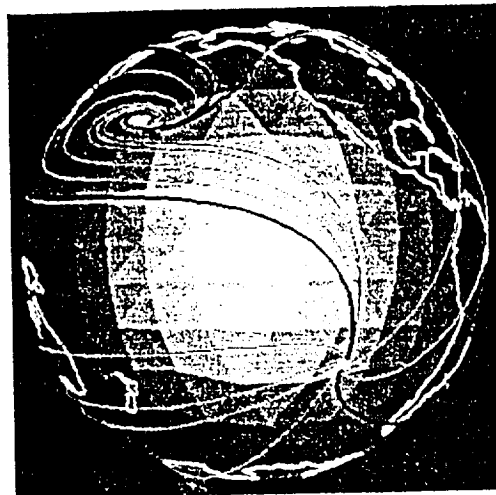
View 1. Level 4
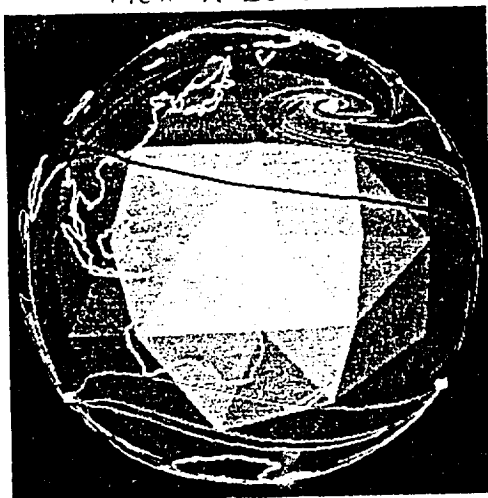
View 2. Level 3
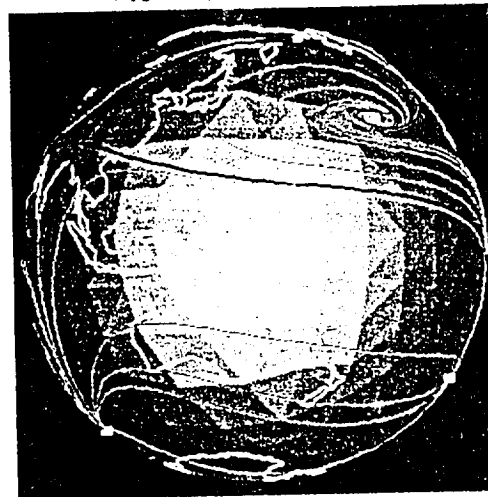
View 2. Level 4
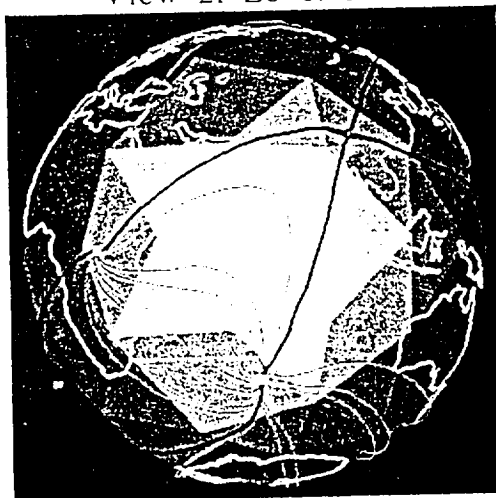
View 3. Level 3
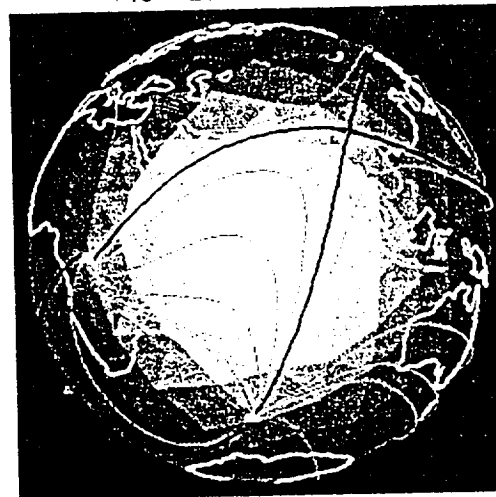
View 3. Level 4

Figure 3. The explicit method applied to a spherical domain
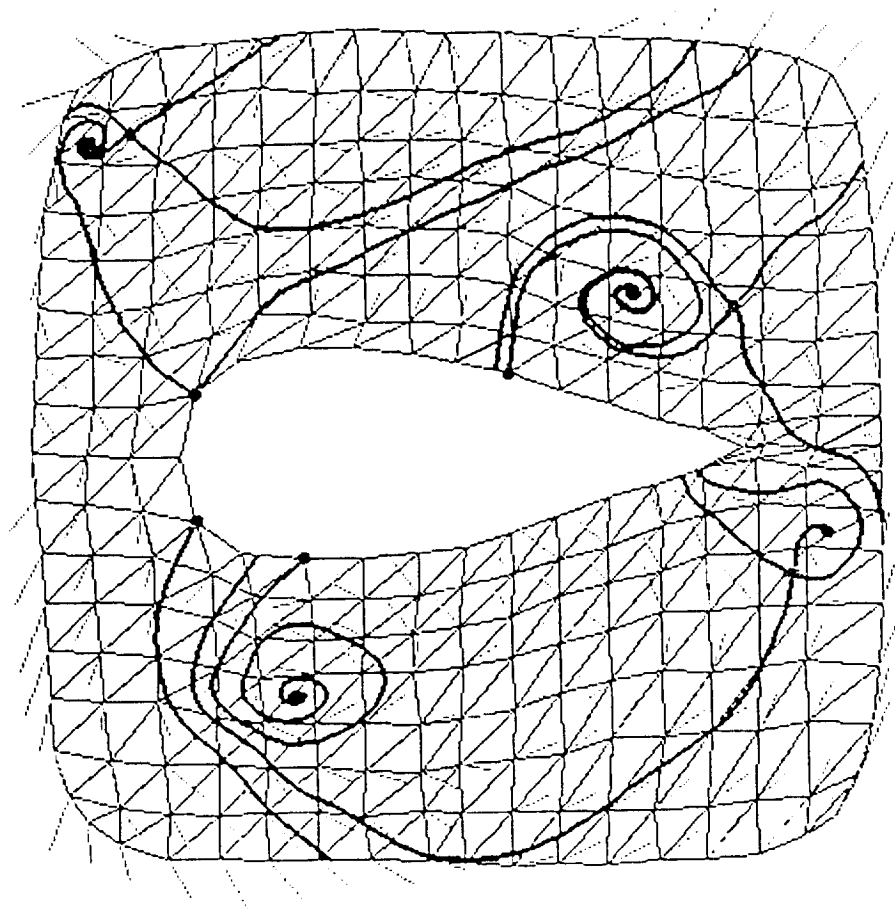
Figure 4. An example with points of attachment and detachment
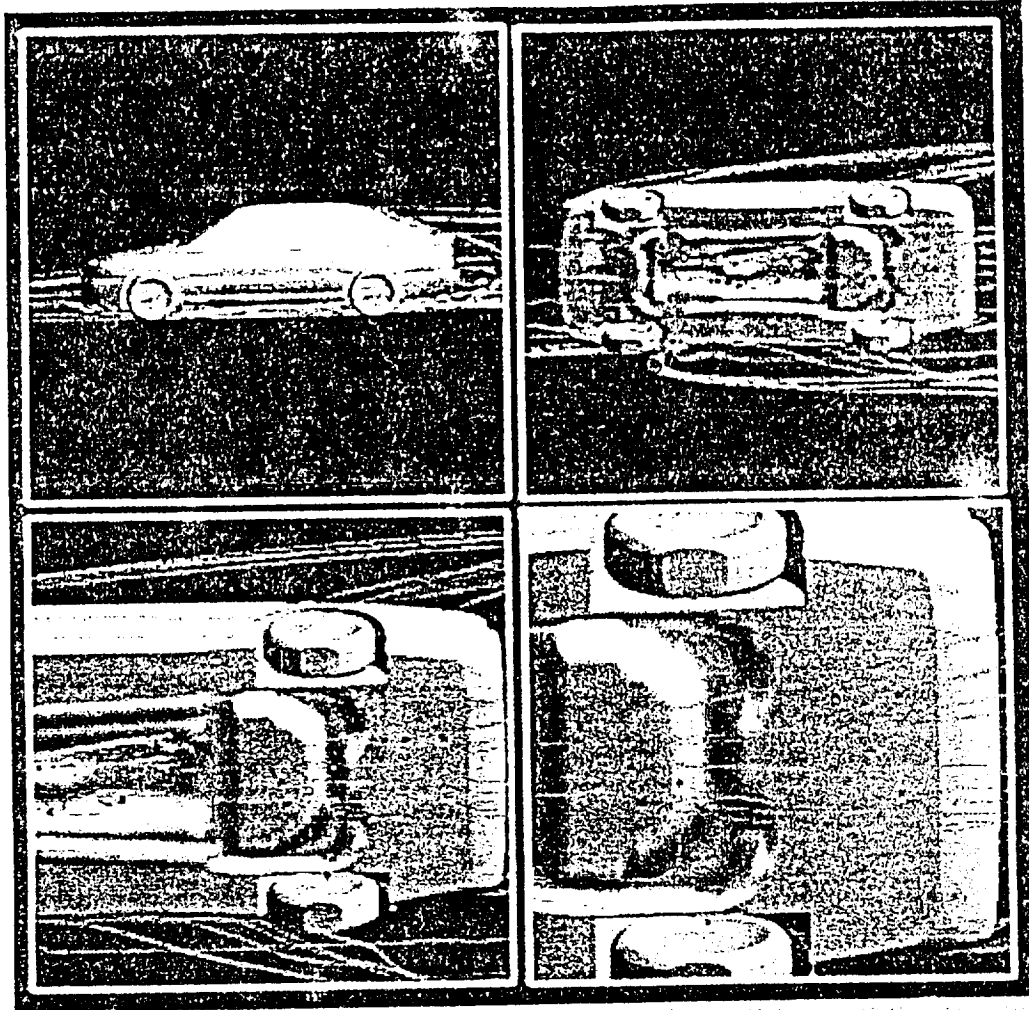
Figure 5. Explicit method applied to 3D data.

We next report on our research progress in multiresolution modeling. Our work in this area can be broken down into two subareas: i) triangular grids with applications to arbitrary domains and ii) curvilinear grids.

First we discuss curvilinear grids. In the original proposal we mentioned the idea of using multiresolution models for parametric curves in this context. The idea is based upon the observation that a curvilinear grid can be viewed as a parametric map and researchers have already developed techniques for using wavelets on parametric curves. See Figure 6.
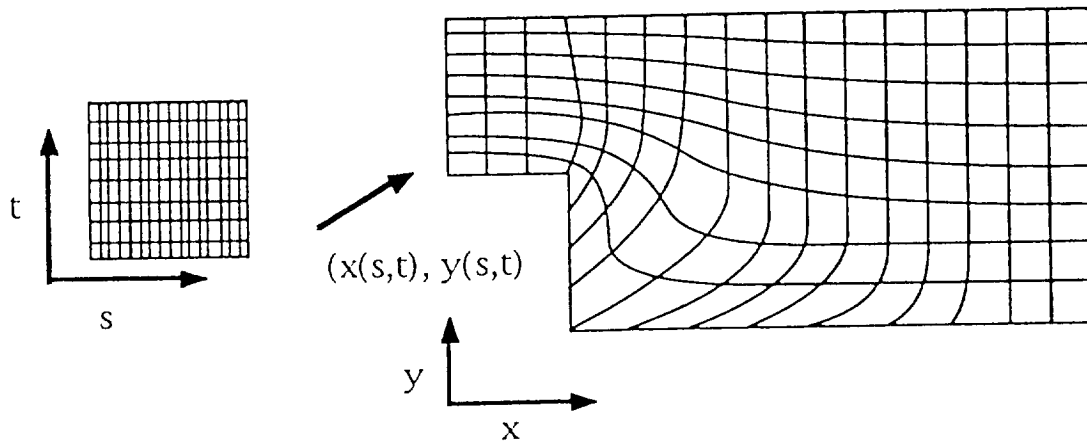

Figure 6. Curvilinear grid as a parametric map

Unfortunately there is a basic problem with this approach and that lies in the fact that not only do you obtain a lower resolution approximation to the flow, but you also get a lower resolution approximation to the boundary of the domain. This means that the domain will be "smoothed down" also. See Figure 7 and note that the inside corner in the lower left region has been rounded off.
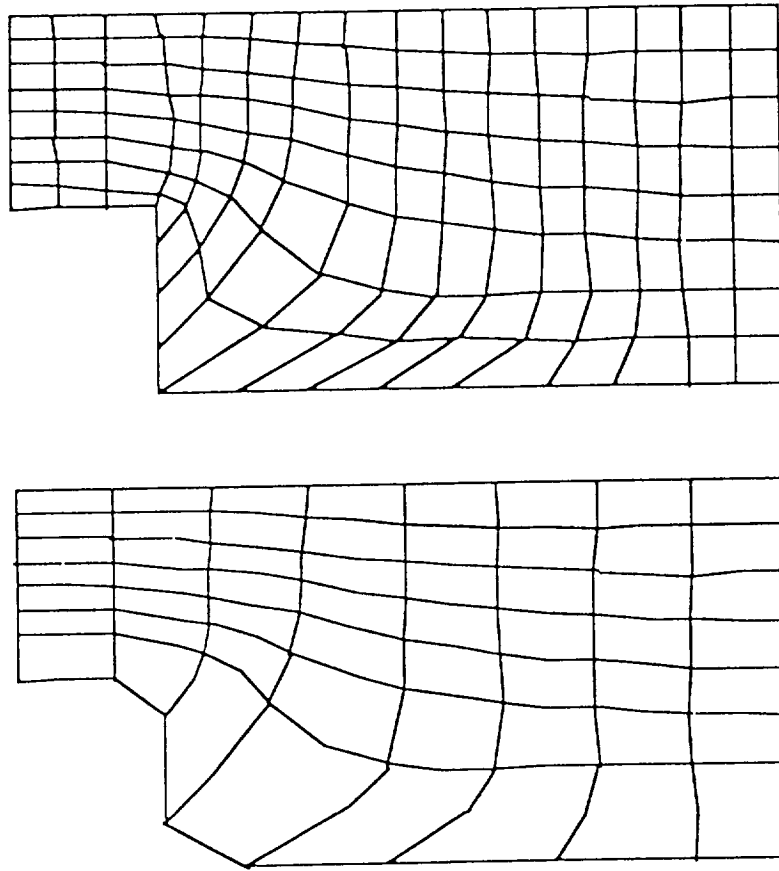
Figure 7. The boundary problem with the parametric wavelet approach

After some consideration, we felt it was rather important to keep the domain intact because often in a flow analysis, the most interesting and important activity occurs near to and as a result of the boundary. In order to preserve the boundary, we have adopted a domain decomposition scheme which is based upon alternate "knot" removal. This is illustrated in Figure 8. Up to now, we have developed and implemented some Haar type of wavelets based upon this type of domain decomposition. In Figure 9 we show an example. This example has both an internal and external boundary and the reader will note that these boundaries stay intact throughout the different levels of decomposition. The example of Figure 10 illustrates the capability to do region selective (lossless) reconstruction. The decomposition allows us to find the best lower resolution approximation and the reconstruction process allows us to add in "detail" when and where it is desired. The possibilities indicated by this rather crude example are really quite exciting!
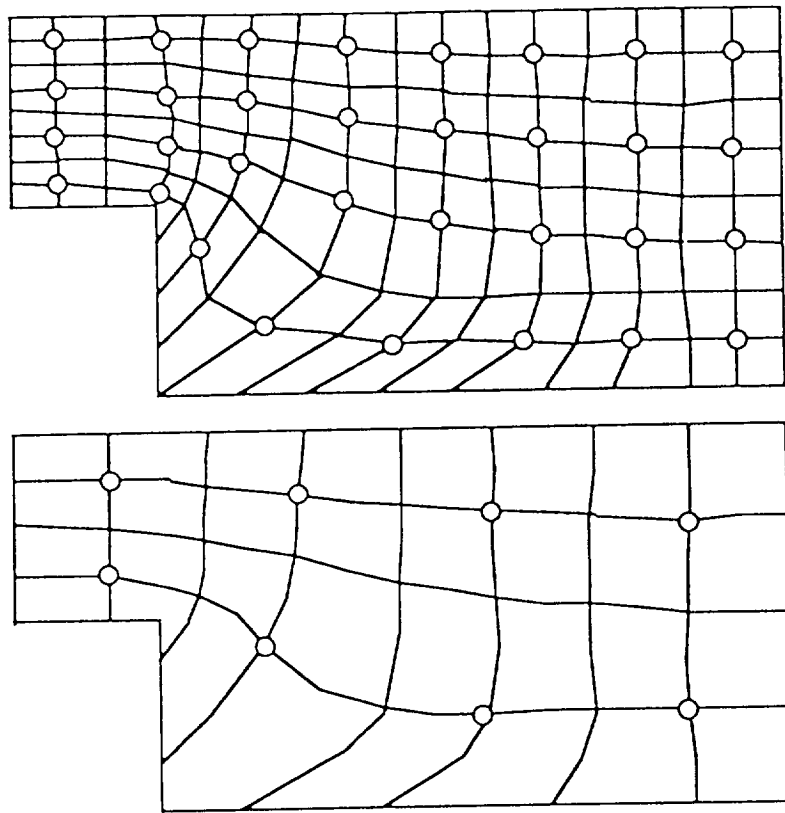
Figure 8. Decomposition by knot removal
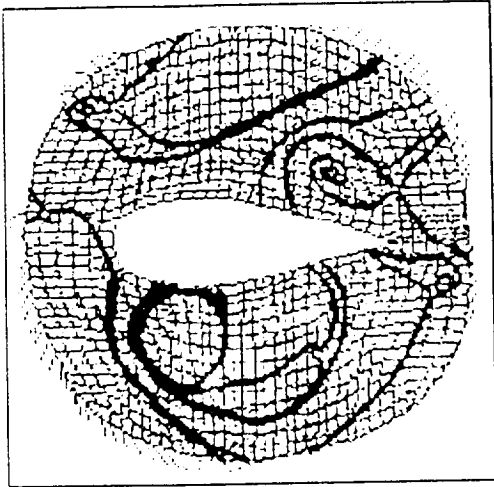
Level 5
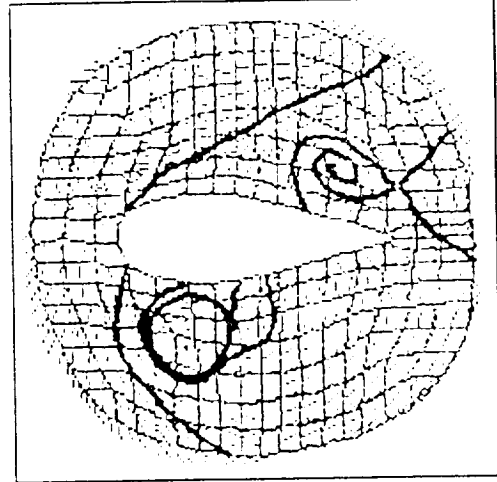
Level 4
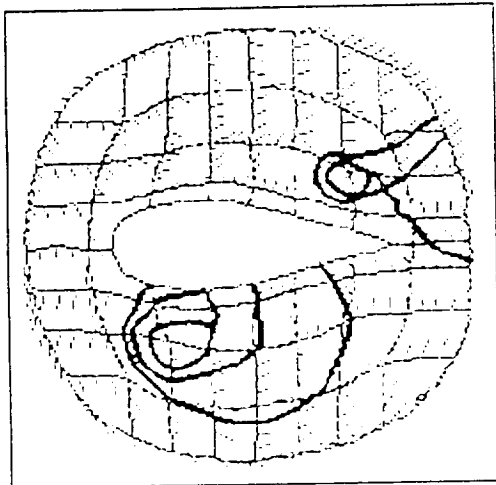
Level 3
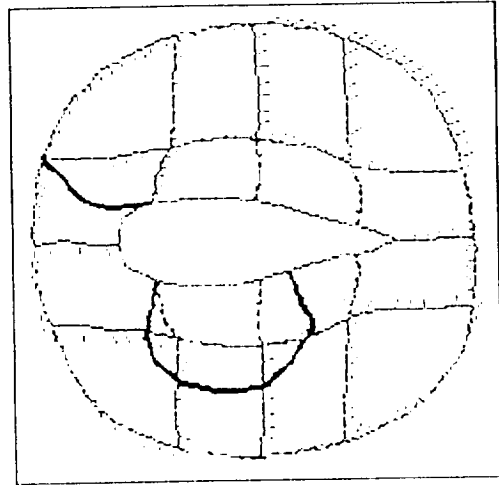
Level 2

Figure 9. Decomposition of flow field over a curvilinear grid.
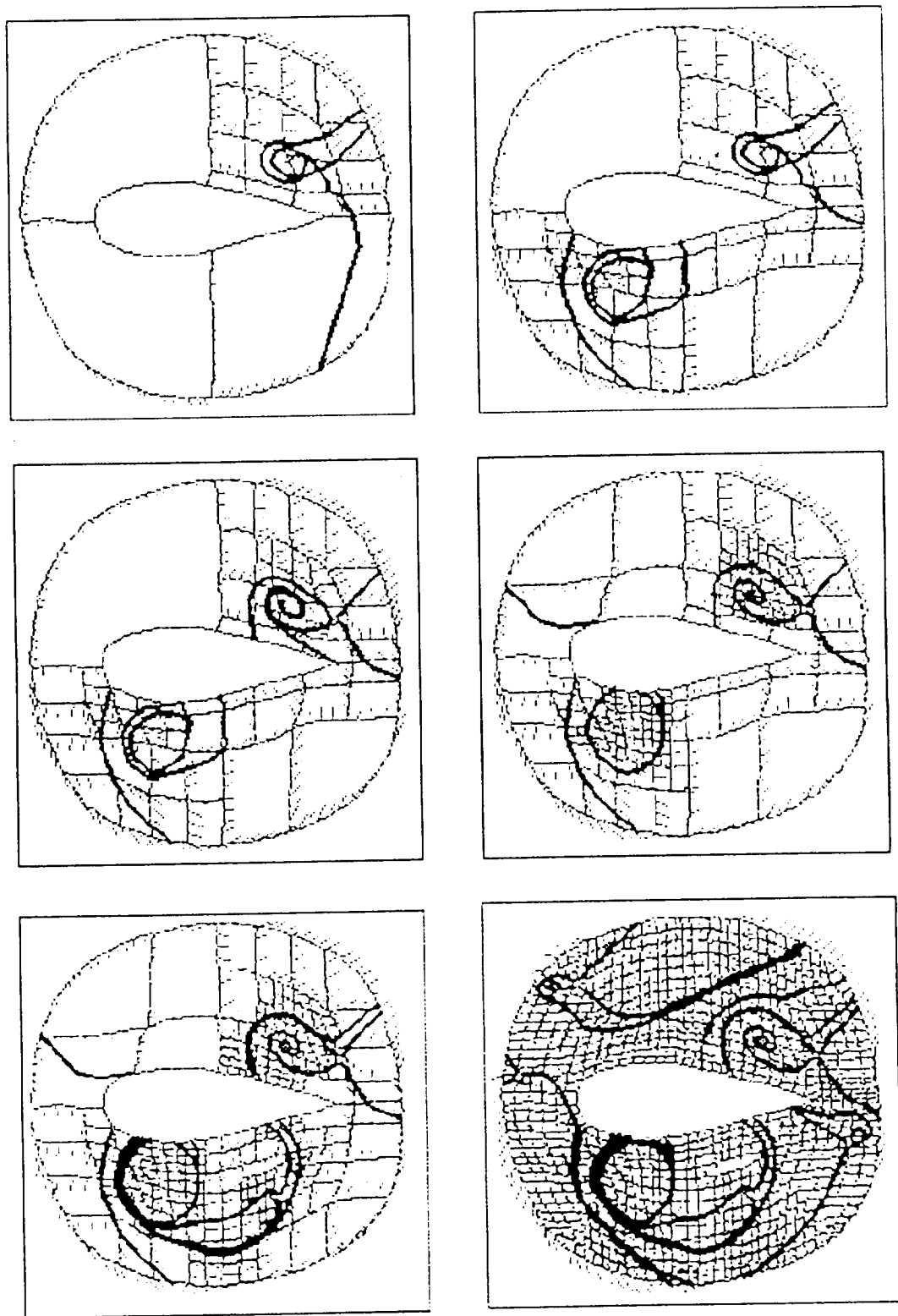
Figure 10. Region specific reconstruction of flow field.

We now discuss our research progress on multiresolution methods for nested triangular grids. We have developed some new Haar type wavelets for subdivision of triangular domains as illustrated in Figure 11. The basic decomposition step is illustrated in Figure 12. The ϕ's are the characteristic functions for the subtriangles and therefore form a basis for piecewise contant functions. The ψ's are the wavelet functions which capture the detail (error) and hopefully they are mutually orthogonal so that we obtain best least squares approximations when we do the wavelet decompositions. This decomposition is simply a change of basis which can be represented by the refinement equations

$$
\begin{bmatrix} \phi(p) \\ \psi_a(p) \\ \psi_b(p) \\ \psi_c(p) \end{bmatrix} = \begin{bmatrix} h_o & h_a & h_b & h_c \\ g_{ao} & g_{aa} & g_{ab} & g_{ac} \\ g_{bo} & g_{ba} & g_{bb} & g_{bc} \\ g_{co} & g_{ca} & g_{cb} & g_{cc} \end{bmatrix} \begin{bmatrix} \phi_o(p) \\ \phi_a(p) \\ \phi_b(p) \\ \phi_c(p) \end{bmatrix} . \tag{1}
$$
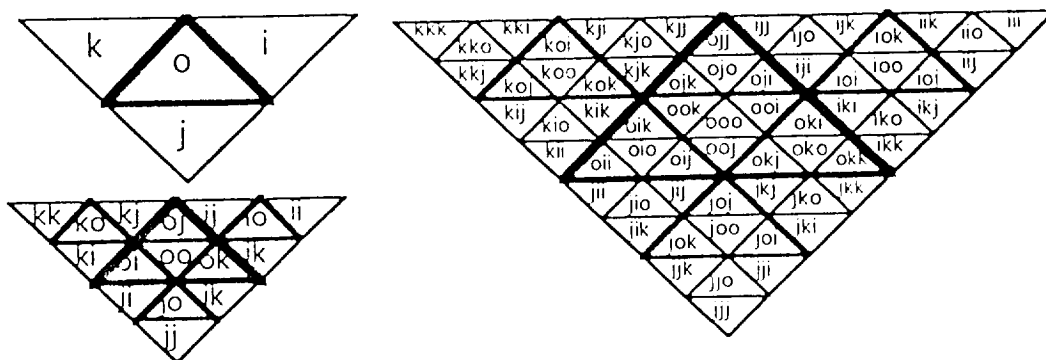
Figure 11. Labeling scheme for triangular subdivision

14

replace

$\lambda \phi$

$+ \gamma_a \Psi_a$ $+ \gamma_b \Psi_b$

$\lambda_o \phi_o + \lambda_a \phi_a + \lambda_b \phi_b + \lambda_c \phi_c$

$+ \gamma_c \Psi_c$
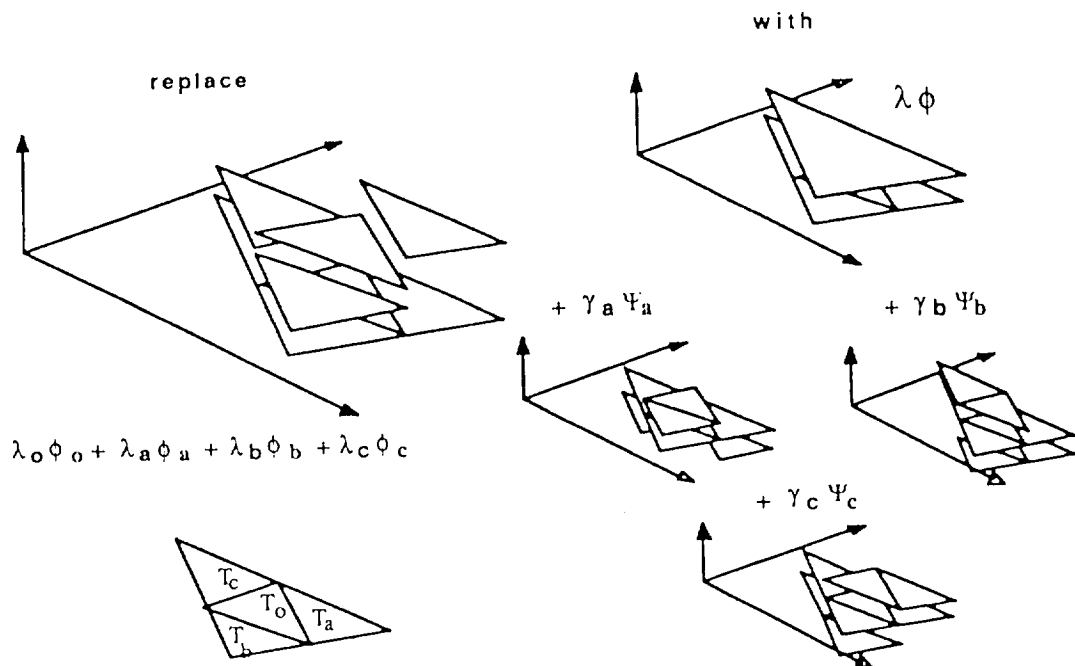
Figure 12. Basic decomposition step

As we have set up things here, we will have defined Haar wavelets for these types of subdivision domains once we specify the h's and g's of the refinement equation (1) above. If the areas of the subtriangles T_o, T_a, T_b and T_c are all the same then it is possible to define Haar wavelets that are mutually orthogonal and affine invariant. If the areas are not the same, then we must settle for biorthogonal wavelets which means that we lose the best approximation properties. One application area where we definitely have subtriangles with different areas is the spherical triangulation obtained by subdivision. Figure 13 illustrates this property.

15

$$\alpha_o \neq \alpha_a \neq \alpha_b \neq \alpha_c$$
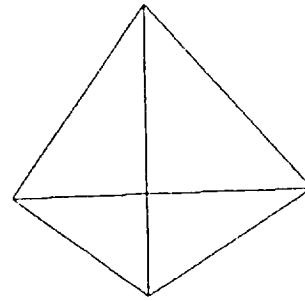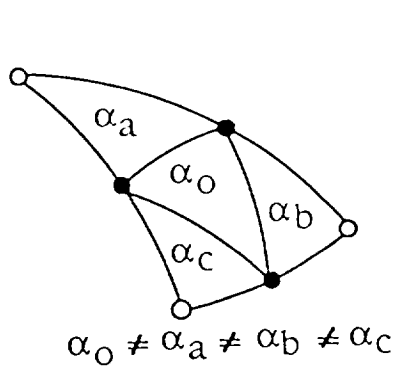
Tetra, Level 1
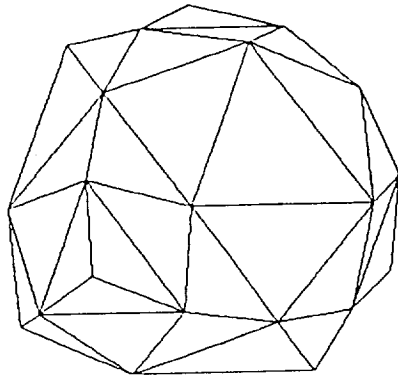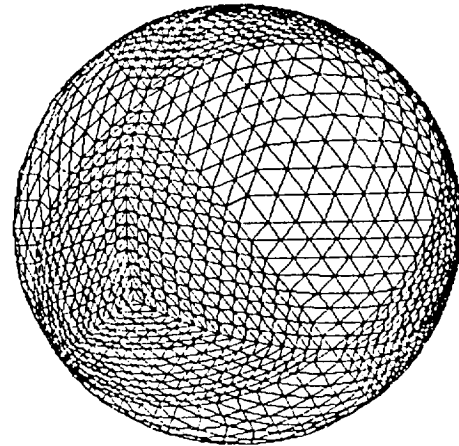
Level 3   Level 6

Figure 13. Spherical Triangular Grid

In a 1995 SIGGRAPH paper, P. Schroeder and W. Sweldens presented some biorthogonal wavelets for spherical triangulations. The definition of their wavelets are given by the refinement equations

$$
\begin{bmatrix} \phi(p) \\ \psi_a(p) \\ \psi_b(p) \\ \psi_c(p) \end{bmatrix} =
\begin{bmatrix}
1 & 1 & 1 & 1 \\
\dfrac{-\alpha}{2(\alpha-\alpha_a)} & \dfrac{\alpha}{2\alpha_a} & \dfrac{-\alpha}{2(\alpha-\alpha_a)} & \dfrac{-\alpha}{2(\alpha-\alpha_a)} \\
\dfrac{-\alpha}{2(\alpha-\alpha_b)} & \dfrac{-\alpha}{2(\alpha-\alpha_b)} & \dfrac{\alpha}{2\alpha_b} & \dfrac{-\alpha}{2(\alpha-\alpha_b)} \\
\dfrac{-\alpha}{2(\alpha-\alpha_c)} & \dfrac{-\alpha}{2(\alpha-\alpha_c)} & \dfrac{-\alpha}{2(\alpha-\alpha_c)} & \dfrac{\alpha}{2\alpha_c}
\end{bmatrix}
\begin{bmatrix} \phi_o(p) \\ \phi_a(p) \\ \phi_b(p) \\ \phi_c(p) \end{bmatrix} .
\tag{2}
$$

We have developed what we consider to be some improvements over these wavelets. These new wavelets are only biorthogonal also, but have the property that when the areas do become the same, the wavelet become mutually orthogonal. They are more nearly orthogonal and so we obtain better approximations with the wavelet

16

decomposition. The reader will note from Figure 13 that for spherical triangular grids these areas quickly become very similar and so for this application these new spherical wavelets will tend towards orthogonal wavelets. The refinement equations for these new wavelets are

$$
\begin{bmatrix} \phi(p) \\ \psi_a(p) \\ \psi_b(p) \\ \psi_c(p) \end{bmatrix} =
\begin{bmatrix}
1 & 1 & 1 & 1 \\
1-\dfrac{\alpha_0^2+\alpha_a\alpha_0}{\Delta} & 1-\dfrac{\alpha_a^2+\alpha_a\alpha_0}{\Delta} & \dfrac{-\alpha_0\alpha_b-\alpha_a\alpha_b}{\Delta} & \dfrac{-\alpha_0\alpha_c-\alpha_a\alpha_c}{\Delta} \\
1-\dfrac{\alpha_0^2+\alpha_b\alpha_0}{\Delta} & \dfrac{-\alpha_0\alpha_a-\alpha_b\alpha_a}{\Delta} & 1-\dfrac{\alpha_b^2+\alpha_0\alpha_b}{\Delta} & \dfrac{-\alpha_0\alpha_c-\alpha_b\alpha_c}{\Delta} \\
1-\dfrac{\alpha_0^2+\alpha_c\alpha_0}{\Delta} & \dfrac{-\alpha_0\alpha_a-\alpha_c\alpha_a}{\Delta} & \dfrac{-\alpha_0\alpha_b-\alpha_c\alpha_b}{\Delta} & 1-\dfrac{\alpha_c^2+\alpha_0\alpha_c}{\Delta}
\end{bmatrix}
\begin{bmatrix} \phi_0(p) \\ \phi_a(p) \\ \phi_b(p) \\ \phi_c(p) \end{bmatrix}
\quad (3)
$$

We have applied our new wavelets to data consisting of a vector field defined over the sphere. In the example of Figure 14, we took a known vector field function and evaluated it to obtain the data. In the left column we show three views of the reconstruction of the wavelet decomposition using only 1% of the coefficients. This means we started with a vector valued function which had 2048 coefficients (one for each triangle). The first time we apply the decomposition equations we obtain a function which is piecewise constant over 512 triangles and plus the 1536 detail (or wavelet) functions. No information is lost, just a change of basis. The next step yields a lower resolution approximation consisting of 128 terms and 384 detail at this level plus the 1536 detail from the first decomposition step. This is continued two more times. This final expansion (of 2048 terms) is scanned and the 20 (1%) functions with the largest coefficients are summed to obtain the partial reconstruction. In the right column we show the reconstruction based upon the largest 409 (20%) coefficients. It is indistinguishable from the original function .

17
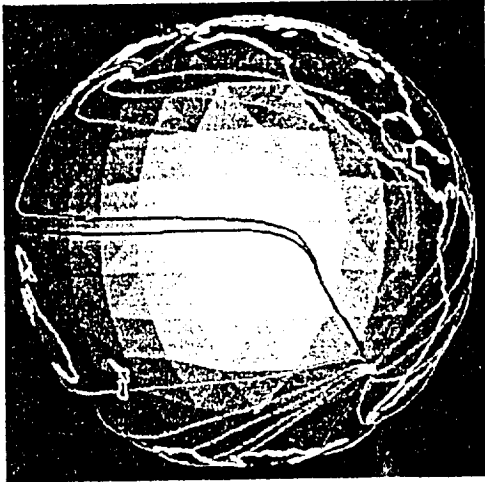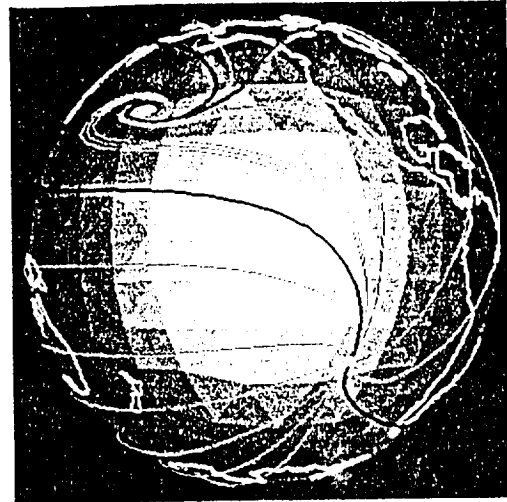
View 1, 1%

View 1, 20%
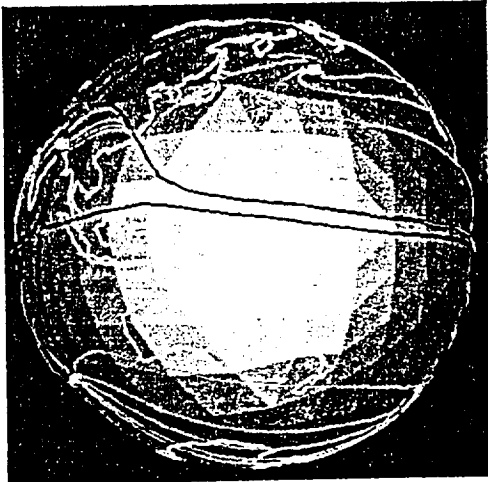
View 2, 1%
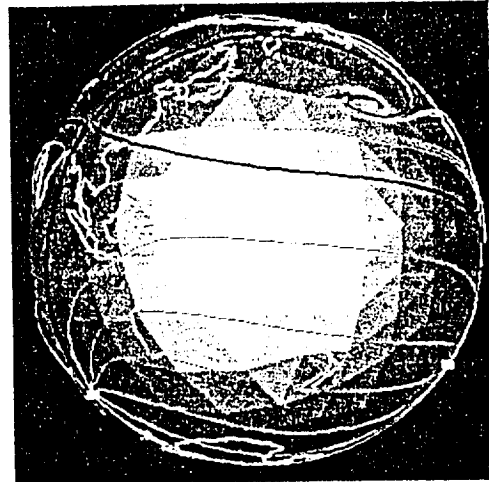
View 2, 20%
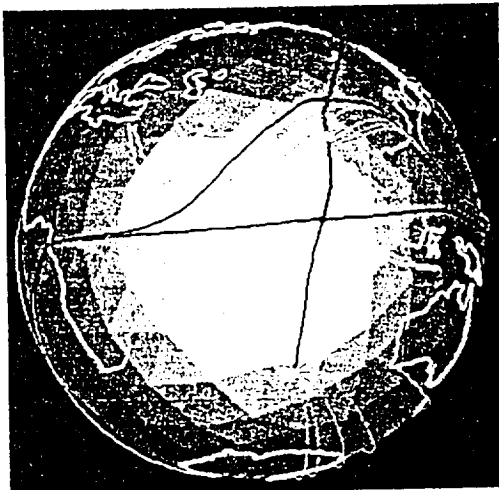
View 3, 1%
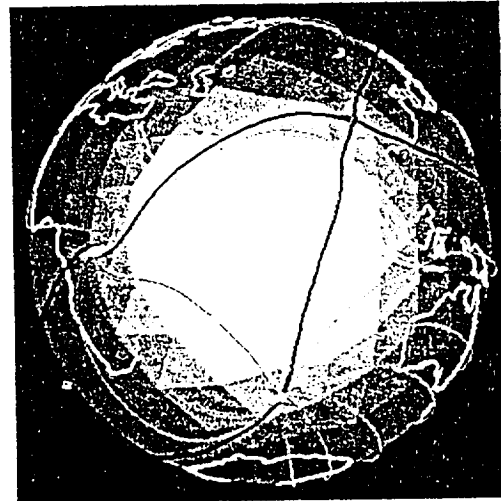
View 3, 20%

Figure 14. Partial (nearly orthogonal) spherical wavelet reconstruction of a flow field defined over a spherical domain.

18

In this next example shown in Figure 15, we applied these new spherical wavelets to some "real" data. This is data we obtained from Roger Crawfis and Nelson Max of Lawrence Livermore National Laboratory. Actually it is simulated data resulting from a global weather model. This data represents one slice in elevation and one time step. The first column shows three different views using a topological graph of the original data. In the second column the reconstruction based upon the 3% largest coefficients is shown. This low resolution approximation allows us to get an overview of the flow without the clutter and detail. As it was shown with the example of Figure 10 it is possible with this type of analysis to zoom in and add detail to any region we wish. Most often wavelets and, in general, multiresolution models are used for compression or efficiency in fly-throughs. The use of these types of models for analysis and visualization of scientific data is potentially very useful and a very exciting area of research.
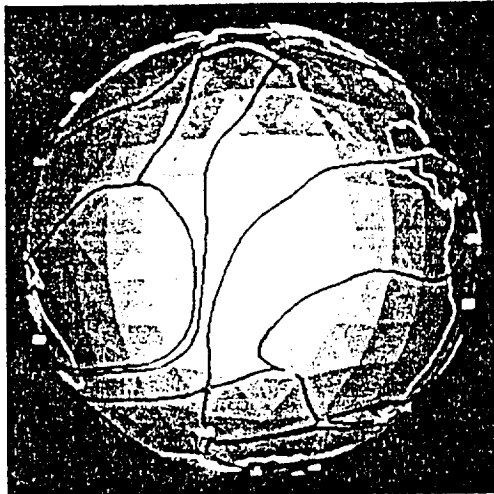
View 1, 100%
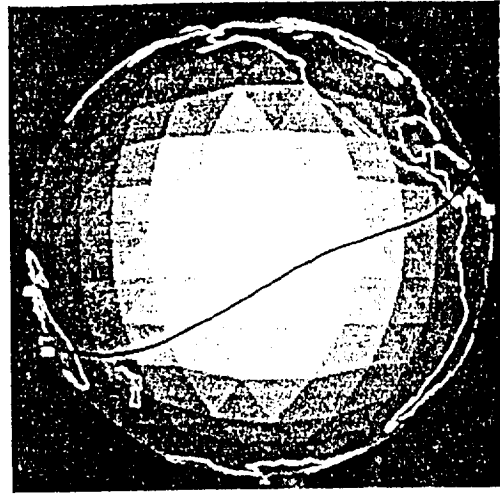
View 1, 3%
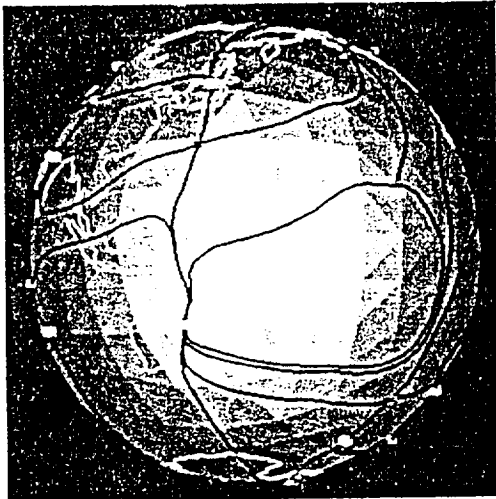
View 2, 100%
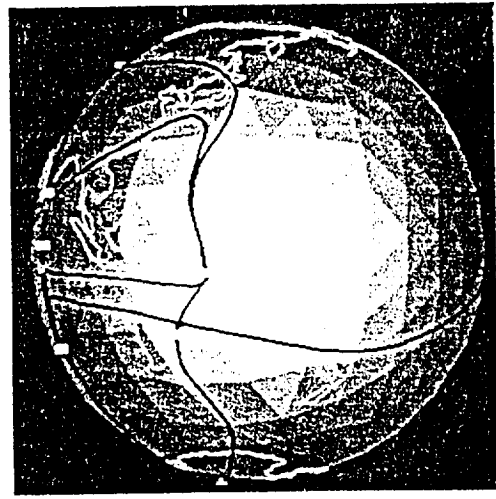
View 2, 3%
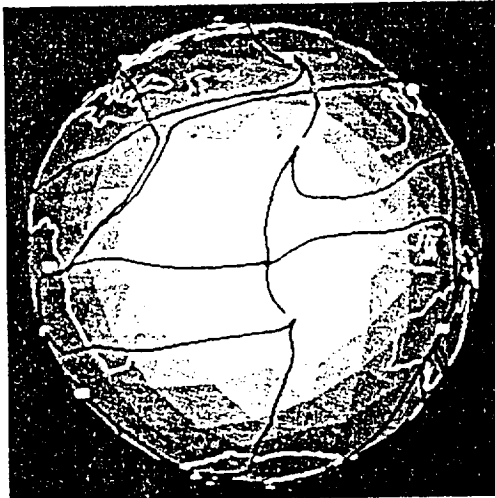
View 3, 100%
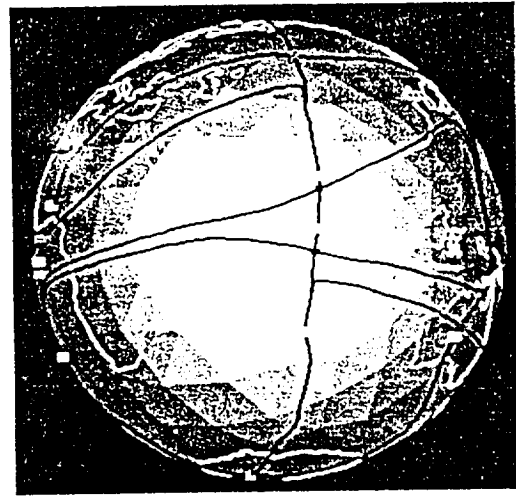
View 3, 3%

Figure 15. Spherical wavelet reconstruction of wind data from global weather model

Statement of Work for Next Year

Concerning work in the area of explicit methods for computing tangent curves, we feel that our algorithms and computer programs are quite robust and efficient at this time. We want to publish this research and make the code available with the hope of getting some feedback. We want to do some further work on comparing the new methods to the conventional stepping methods. As we have mention before, these new methods allow errors to be bounded and controlled while all other methods only can at best estimate errors. We feel that this is important in general and in particular for linking algorithms for topological methods. We hope to determine just how critical this issue is. Even though we showed a 3D example in Figure 5, this was really just preliminary work. We need to do a through and complete job on the case analysis based upon eigenvalues. Also as, as we pointed out in the 2D work, the approach which uses an implicit representation for the tangent curve and a parametric representation for the edge has some definite advantages. We need to do the mathematics of finding implicit representations of the 3D parametric tangent curves. Once all the mathematics is done, we need to develop and implement the algorithms. Linking algorithms for topological methods require the definition of points of attachment and detachment. As we mentioned, in the past this has not been dealt with very well. For our linearly varying fields in 2D, can precisely define and compute these special critical points. The same theory for 3D needs to be developed and we intend to do this.

Concerning work in the area of multiresolution methods for curvilinear grids, we want to develop some methods which are higher order and have more continuity than the simple Haar wavelets that we have developed so far. We will first do this for 2D flows, starting with the development of piecewise linear wavelets over the nested decompositions we already mentioned. Also, we want to extend the basic 2D Haar wavelets to 3D. This requires the development of a 3D knot removal scheme leading to the nested, cellular decomposition of the domain. In principle this should not be much of a problem, but there are some details with the tetrahedrization of cells that we are concerned about but we feel that they can be dealt with.

Concerning our work next year in the area of multiresolution models over triangular grids, we need to extend these basic Haar methods to higher order and higher continuity. Also we would like to extend this work to 3D. A critical component of the 2D

implementation was a clever triangle naming scheme which allowed neighboring triangles to be quickly and easily determined. To some this might be considered just an implementation detail, but to us it was very critical to the entire algorithm. We need to develop a 3D version of the labeling scheme and then proceed to develop the basic refinement and decomposition equations for the Haar wavelets defined over nested tetrahedral subdivisions. Just as the 2D triangular methods were extended to a spherical domain, we should be able to extend the 3D version to tetrahedral approximation of any three dimensional manifold. This would include SO(3) (the space of orientations) and could have some interesting implications on image interpolation and its use in VRML applications.

In conclusion, we give an outline of the planned research activities for next year:

- Explicit Methods

  Publish papers, distribute algorithms, solicit feedback
  Extend to 3D
  > Implicit representation of 3D parametric curves
  > Definition of attachment and detachment curves on interior boundaries
  > Tetrahedrization of 3D curvilinear grids

- Multiresolution over Curvilinear Grids

  Two-dimensional
  > Develop higher order (continuity) wavelets
  > Apply techniques to many and various data sets

  Three dimensional
  > Develop knot removal algorithm and software for 3D curvilinear grids. Develop Haar wavelets over these grids.
  > Develop higher order (continuity) wavelets

- Multiresolution methods for nested triangular grids

  Two-dimensional
  > Develop higher order (continuity) wavelets
  > Apply to spherical data and flow over other domains

  Three dimensional
  > Develop labeling scheme and basic Haar wavelets
  > Apply to image interpolation problem for VRML

Budget

We are requesting funds for the principal investigator as follows:

> Gregory M. Nielson
>> 2 summer months
>> (see budget sheet for amounts)

We are requesting funds for two students:

> Two ASU Graduate Students
>> 9 months half time, 3 months full time
>> (see budget sheet for amounts)

We are requesting funds in the operations category as explained on the budget sheet

ESTIMATED BUDGET

PERIOD OF PERFORMANCE: January 1,1995 through December 31, 1997

						Year 1	Year 2	Year 3	Summary
I.	SALARIES & WAGES								
	A. PI: Nielson		0.00	pm/AY +	2.00 pm/Sum	S16,610	S17,607	S18,663	S52,880
	B. Co-PI:		0.00	pm/AY +	0.00 pm/Sum	S0	S0	S0	S0
	C. Co-PI:		0.00	pm/AY +	0.00 pm/Sum	S0	S0	S0	S0
	D. Co-PI:		0.00	pm/AY +	0.00 pm/Sum	S0	S0	S0	S0
	E. Postdocs	0 @	0.00	pm/CY		S0	S0	S0	S0
	F. Technicians	0 @	0.00	pm/CY		S0	S0	S0	S0
	G. Graduate Associates	2 @	9.00	pm/AY +	6.00 pm/Sum	S35,020	S36,050	S37,767	S108,837
	H. Graduate Assistants	0 @	0.00	pm/AY +	0.00 pm/Sum	S0	S0	S0	S0
	I. Undergraduates	0 @	0.00	pm/AY +	0.00 pm/Sum	S0	S0	S0	S0
	J. Secretary	0 @	0.00	pm/CY		S0	S0	S0	S0
	TOTAL					S51,630	S53,657	S56,430	S161,717
II.	FRINGE BENEFITS					S4,153	S4,402	S4,666	S13,221
	A. Faculty at	25%				S0	S0	S0	S0
	B. Staff at	30%				S1,051	S1,082	S1,133	S3,266
	C. Students at	3%							
	TOTAL					S5,204	S5,484	S5,799	S16,487
III.	TRAVEL					S0	S0	S0	S0
IV.	OPERATIONS								
	A. Consultants					S0	S0	S0	S0
	B. Publication/Page Charges					S0	S0	S0	S0
	C. Photocopy, telephone, postage, misc.					S500	S500	S500	S1,500
	D. Material & Lab Supplies/Equipment Use Fees					S1,000	S1,000	S1,000	S3,000
	E. Computer Software					S200	S0	S0	S200
	F. Lab Equipment under S500					S0	S0	S0	S0
	G. Subcontracts					S0	S0	S0	S0
	H. Participant Support Costs					S0	S0	S0	S0
	I. Tuition	0 @	S1,895 per AY	(4% escalation)		S0	S0	S0	S0
	J. Student Stipends					S0	S0	S0	S0
	K. Other					S0	S0	S0	S0
	TOTAL					S1,700	S1,500	S1,500	S4,70
V.	CAPITAL EQUIPMENT					S0	S0	S0	S
VI.	TOTAL DIRECT COSTS					S58,534	S60,641	S63,729	S182,90
VII.	INDIRECT COSTS								S95,7
		Year 1	52.0%	MTDC		S30,438			
		Year 2	52.5%	MTDC			S31,837		
		Year 3	52.5%	MTDC				S33,458	
VIII.	TOTAL PROJECT COSTS					S88,972	S92,478	S97,187	S278,6